AN INVESTIGATION OF SELECTED AS-CAST Pt-Cr-Nb ALLOYS

F.M.L. Mulaudzi[1,2], L.A. Cornish[1,2] and M.J. Witcomb[2,3]

[1]*School of Chemical and Metallurgical Engineering, University of the Witwatersrand, Johannesburg, South Africa*
[2]*DST/NRF Centre of Excellence for Strong Materials, University of the Witwatersrand, Johannesburg, South Africa*
[3]*Electron Microscope Unit, University of the Witwatersrand, Johannesburg, South Africa*

ABSTRACT

Superalloys based on platinum-group metals (PGMs) are being developed for high temperature applications, and have a two-phase microstructure comprising ordered precipitates in a matrix analogous to the γ/γ' microstructure of the nickel-based superalloys, the phases being (Pt) and Pt_3Al. These Pt-based superalloys have the potential to substitute Ni-based superalloys (NBSAs) for even higher temperature applications, because of their higher melting point. Running turbines at higher temperatures increases their effeciency, meaning less fuel is needed. Although Pt-based alloys are unlikely to replace all NBSAs on account of both higher price and higher density, they are aimed at the highest application temperature components. Currently, the optimum alloy is $Pt_{84}:Al_{11}:Ru_2:Cr_3$. Niobium (Nb) is a possible addition to increase the alloy's melting point, but only binary phase diagram data are available. Although work has been done on the Pt-Al-Nb ternary system, there are no reported data for the Pt-Cr-Nb system.

As-cast samples of the Pt-Cr-Nb system have been investigated using scanning electron microscopy with energy-dispersive X-ray spectroscopy (SEM-EDX), and X-ray diffraction (XRD). The results have been used to plot a solidification projection and all binary phases have been found to extend into the ternary, with (Cr) having the least extension of ~2 at.%. The (Pt), ~$NbCr_2$, (Nb), ~Nb_3Pt, ~$NbPt_2$ phases extend around 20 at.% into the ternary. Five ternary phases have been indentified at: ~$Nb_{17}:Cr_{64}:Pt_{19}$; ~$Nb_{28}:Cr_{55}:Pt_{17}$; ~$Nb_{30}:Cr_{30}:Pt_{40}$; ~$Nb_{45}:Cr_{27}:Pt_{28}$; ~$Nb_{40}:Cr_{18}:Pt_{42}$. Hardness tests for the alloys have been undertaken, and mechanical behaviour of the individual phases was identified, and hence the suitability as alloys components.

Keywords: Phase diagram, Nb-Cr-Pt system, scanning electron microscopy, X-ray diffraction, Hardness

1. Introduction

Nickel-based superalloys (NBSAs) have excellent properties, but they have reached their temperature capability limit for operation in turbine engines, despite advanced processing technologies like single crystal technology, air cooling and thermal barrier coatings [1987Sim]. Currently, the maximum temperature at which NBSAs operate is ~1100°C, which is 85% of the melting temperature [1987Sim]. If the operating temperature could be increased to higher temperatures, this would improve the efficiency of turbine engines and enable greater thrust, improved fuel efficiency and reduced pollution. Therefore, there is interest in developing similar structured alloys based on an alloy with a higher melting point which can be used at temperatures of ~1300°C and above. Platinum has been selected as the base material for these alloys because of its similarity to Ni in fcc structure and similar chemistry, higher melting point (1769°C for platinum; 1455°C for nickel) and improved oxidation resistance [2000Wol].

There is one important difference between the NBSAs and the Pt-based alloys. There is only one form of Ni_3Al, whereas the phase Pt_3Al has at least two forms [1990Mas], and the more desirable high temperature $L1_2$ structure needs to be stabilised. There are one, if not two, lower temperature forms. One is the distorted $L1_2$ structure DO′c, which originates from a martensitic-type transformation at ~400°C [1986Mis]. A modified DO′c structure has also been identified [2007Dou].

Pt–based alloys have been studied at Mintek and have microstructures that are analogous to the γ/γ′ ((Ni)/~Ni_3Al) microstructure of the NBSAs [2000Wol, 2001Hil, 2002Cor, 2003Cor and 2003Süs1], although the precipitate volume fraction (~30%) was not as high as in the Ni–based Superalloys (~70%). These Pt–based alloys have the potential to substitute NBSAs in extreme applications, because of their higher melting points and good corrosion resistance. Although Pt–based alloys are unlikely to replace all NBSAs on account of both higher price and higher density, it is likely that they can be used for the highest application temperature components. The ternary alloys have mechanical properties which are better than those of the Ni– and Co–based superalloys, higher than conventional solid–solution strengthened Pt–based alloys, and comparable with mechanically alloyed ferritic oxide–dispersion–strengthened (ODS) alloys [2002Süs2]. The best alloy composition so far is Pt_{84}:Al_{11}:Ru_2:Cr_3, and its oxidation resistance is better than the original ternary alloys [2001Süs]. It has been shown that the quaternary and ternary alloys have room temperature tensile properties similar to that of other high temperature alloys [2004Süs2]. However, the quaternary alloy needs further optimisation in terms of heat treatments and additional alloying to obtain the best properties, and this is ongoing [2008Sho]. In order to decrease both the density and the cost of the alloys, other additions are being considered. Niobium is potentially useful because its high melting point should help to increase the melting point of the alloys.

As well as developing the alloys, a thermodynamic database is being built to facilitate the further development of the alloys. This work needs phase diagrams of all the component systems, as well as thermodynamic data. Currently, the database comprises Pt-Al-Cr-Ru, and it is being extended to contain niobium [2008Ukp]. Although the binary systems have been published [1990Mas], there were no published ternary systems for the Pt–Al–Cr–Ru system at the beginning of the programme. Experimental phase diagram work has now been done on the ternary systems: Al–Cr–Ru [2000Com1, 2000Com2, and 2001Com], Pt–Al–Ru [2003Pri], Pt–Cr–Ru [2002Süs1, 2003Süs1, 2003Süs2, 2004Süs1], Pt–Al–Cr [2003Süs3, 2008Süs], Pt–Al–Co [2003Cho], Pt–Al–Ni [2003Gla] and Pt–Al–Nb [2006Ndl, 2007Ndl].

In investigations in Germany [2004Vor, 2005Wen], alloys with 10–13 at.% Al, 3–6 at.% Cr, 6 at.% Ni and balance Pt showed similar two–phase microstructures to the Pt–Al–Cr–Ru alloy and lattice misfits similar to conventional NBSAs. The microstructures were optimised by heat treating.

The quaternary Ir–Nb–Pt–Al system has been studied by Huang *et al.* [2003Hua, 2004Hua1, 2004Hua2, 2005Hua], and it has been found that an fcc/$L1_2$ two–phase structure exists in both Pt–Al and Ir–Nb binary systems and the lattice parameters of $L1_2$ phases (Ir_3Nb and Pt_3Al) are similar. The solubility of Ta in the $L1_2$–Pt_3Al phase was reported to be about 5 at.%; accordingly, a similar solubility is expected for Nb in $L1_2$–Pt_3Al. No phase transformation was detected [2004Hua2, 2005Hua], which indicated that the $L1_2$–Pt_3Al structure was stabilised at room temperature. The phase stabilisation of the $L1_2$–Pt_3Al structure was attributed to the Nb addition, according to the investigation on Pt–Al–Nb ternary system.

Thus, Nb has been identifed as stabilising the beneficial $L1_2$ Pt_3Al phase, as well as for increasing the melting point, and reducing the cost and density by the substitution of some of the platinum. Considering the addition of Nb to these alloys, the system becomes more complex and there are more ternaries which need to be investigated. Pt–Al–Nb has already been studied [2006Ndl, 2007Ndl]. The next system chosen was Pt-Cr-Ru, and this work was to derive the Pt-Cr-Nb phase diagram, since no data were available in the literature.

2. Previous phase diagram work

The component binary systems [1990Mas] are mostly well-established for the Pt-Cr-Nb system, although the Cr-Pt has recently been updated using thermal conductivity measurements [2005Zha], and Cr-Nb was updated for the two $NbCr_2$ Laves–type phases: high temperature hexagonal $MgZn_2$–type and low temperature cubic $MgCu_2$–type [1992Tho, 1993Oka]. The phase diagrams are given in Figures 1 to 3.

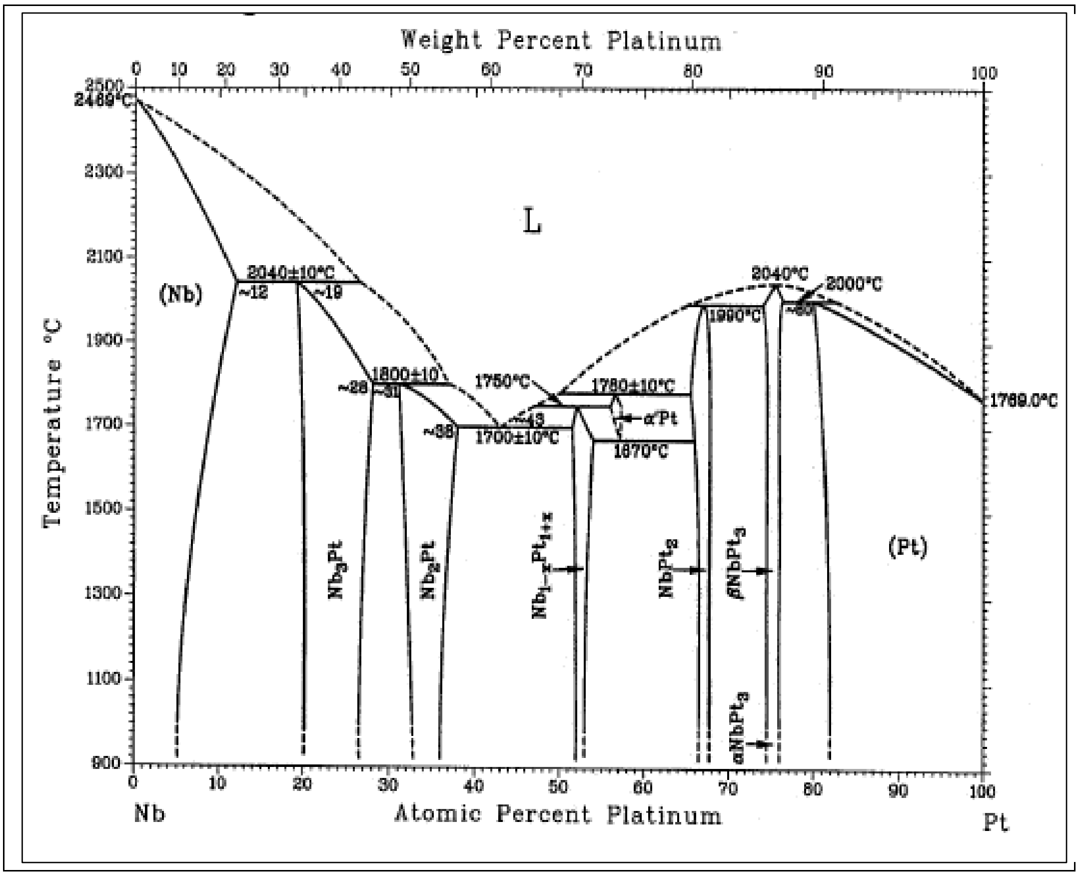

Figure 1. Nb–Pt equilibrium phase diagram **[1990Mas].**

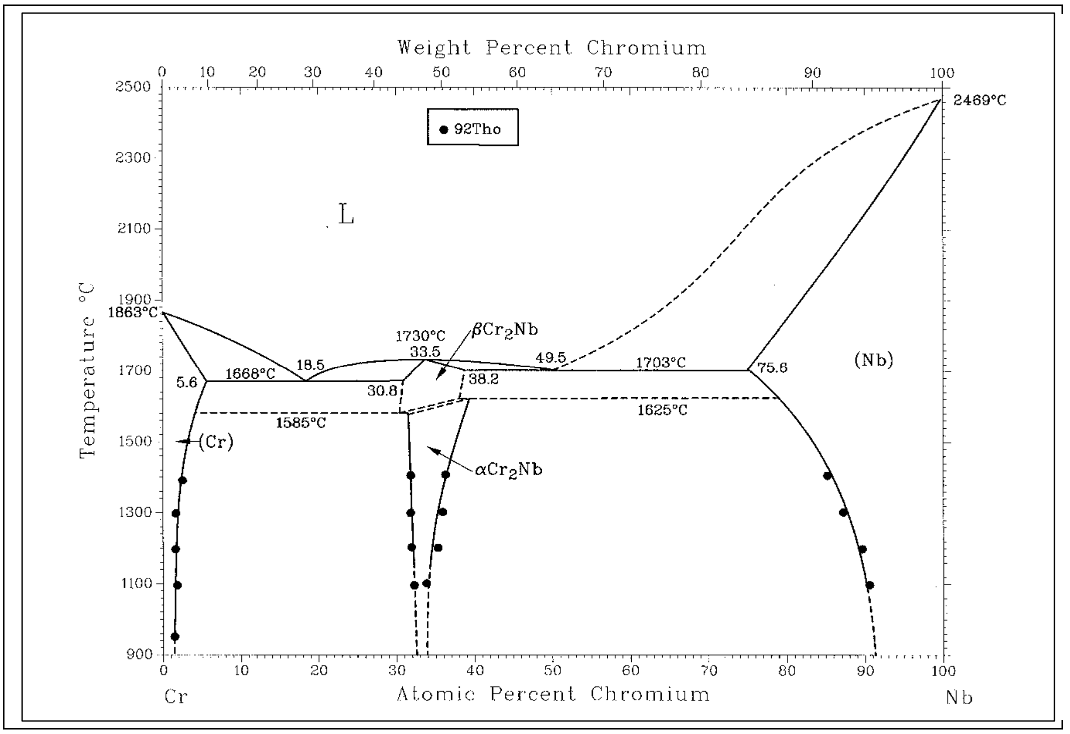

Figure 2. Cr-Nb phase equilibrium diagram **[1992Tho, 1993Oka].**

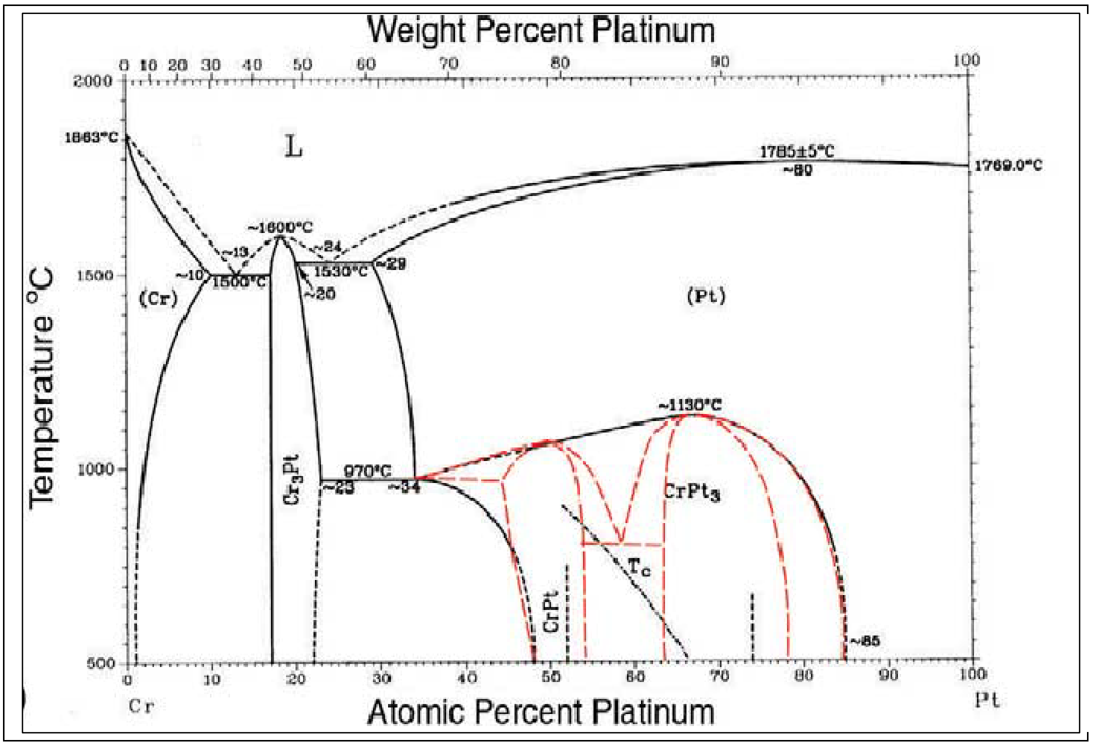

Figure 3. Cr–Pt equilibrium phase diagram **[2005Zha].**

The Nb–Cr–Pt ternary phase diagram was not published in the available literature.

3. Experimental Procedure

The initial six sample compositions were selected to be as far away from each other and the binaries as possible to give an overview of the phases in the system. After these were characterised, subsequent samples were chosen to fill in the gaps in the information. The samples were made by mixing weighed elements of at least 99.95% purity in the required proportions, and the ~2g samples were produced by arc–melting under an argon atmosphere, using Ti as an oxygen–getter. These samples were turned and remelted several times to improve homogeneity.

The samples were sectioned and prepared for metallography in the as–cast condition. Each sample was mounted in conductive resin and ground to 1200 grit on SiC paper, then polished on 6μm , 3μm and 1μm diamond cloths. Samples were completed using an oxide polishing (OP–S) system, by which polishing is achieved through a combination of chemical treatment and gentle abrasive action.

The microstructures were examined using a LEO-1525 scanning electron microscope (SEM) with energy-dispersive X-ray spectroscopy (SEM-EDX), in mainly the backscattered electron (BSE) mode for phase contrast by average atomic number. During EDX analysis, at least five spot analyses were taken from each phase, but where there was a small size phase area, the best analysis was taken, taking into account the other measurements and the size of the area.

The X–ray diffraction (XRD) was undertaken on a Phillips (PW1830) X–ray diffractometer, using a Cu–Kα source, with 0.02^{o} step size and 1.0s scan step time. Phases were identified by comparison with the ICDD database.

After studying the microstructures, Vickers macrohardness measurements were conducted on all the samples using a Vickers Ltd. Vicker's instrument. A 5 kg load was used, with at least five measurements taken randomly in homogeneous samples to obtain an average hardness value. In inhomogeneous samples, indentations were placed selectively. Care was taken to ensure that each individual indentation was more than two diagonals away from other indentations. In all cases, the load was applied for ~15 seconds.

Macrohardness indentations were photographed using a Nikon FX-35A digital camera connected to the Nikon optical microscope, with Motic Images Plus 2.0 ML software. The alloys were categorised by slip modes, and cracking behaviour.

4. Results

4.1 Phase diagram investigation

All alloys were only studied in the as-cast condition. The EDX analyses for the overall alloy compositions and the phases were used in Figure 24, and the overall eutectic analyses are given in Table 1. Where no errors are given, one analysis was selected as the best (usually because all the regions were small). The phases were mostly confirmed by X-ray diffraction (XRD), and an example is given in Figure 4. Some phases were not in the ICDD database (~$Nb_{1-X}Pt_{1+X}$ and ~Nb_2Pt), and these will be modelled in the future.

Table 1. EDX analyses of the eutectics.

Alloy No and composition (at.%)	Element	Eutectic composition (at.%)	Eutectic
5	Nb	44.4	
~$Nb_{42.4}$:$Cr_{42.6}$:$Pt_{15.0}$	Cr	39.4	~$NbCr_2$ + ~Nb_2Pt
	Pt	16.3	
6	Nb	48.3±3.3	
~$Nb_{69.9}$:$Cr_{16.1}$:$Pt_{14.0}$	Cr	45.0±4.2	~Nb_3Pt + ~$NbCr_2$
	Pt	6.7±1.1	
10(d)	Nb	44.2±0.8	
~$Nb_{42.5}$:$Cr_{38.6}$:$Pt_{18.9}$	Cr	37.8±1.3	~$NbCr_2$ + ~Nb_2Pt
	Pt	18.0±0.5	
	Nb	44.3	
	Cr	35.2	~$NbCr_2$ + ~Nb_2Pt + τ4
	Pt	20.5	

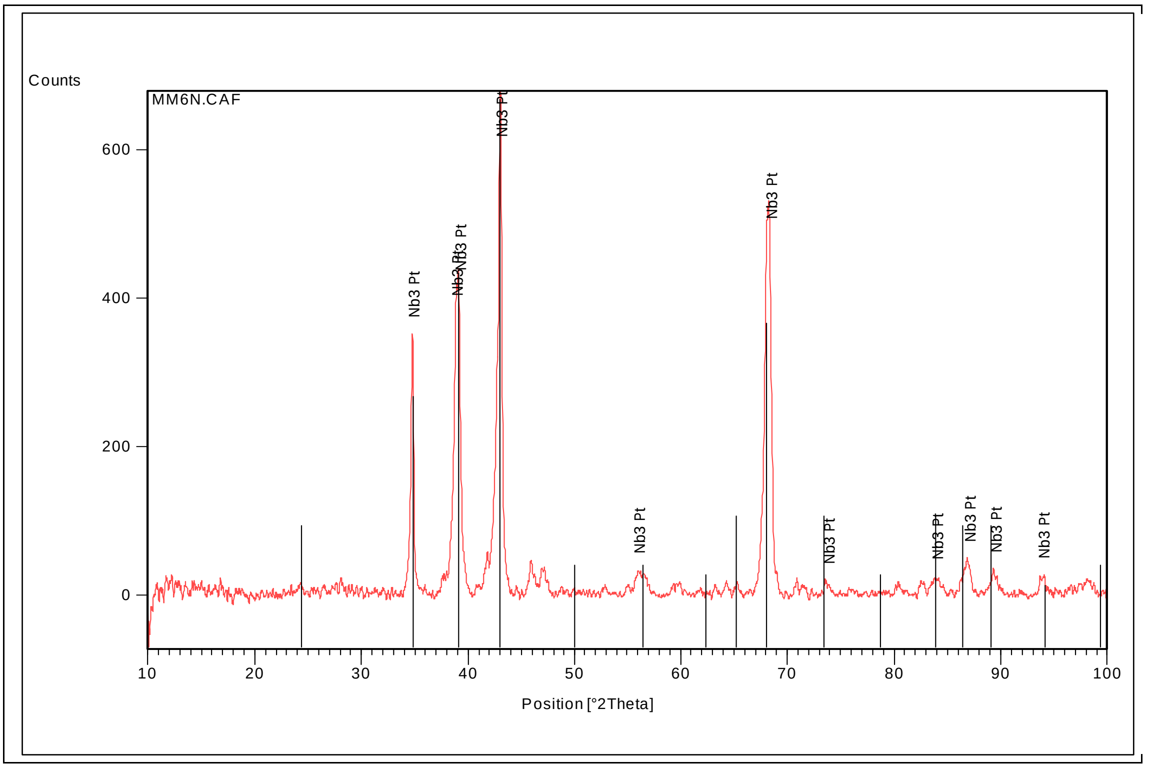

Figure 4. XRD pattern of nominal Nb_{70}:Cr_{15}:Pt_{15} in the as-cast condition, showing black ~Nb_3Pt peaks.

Nominal Nb_{15}:Cr_{15}:Pt_{70}, Sample 1 and Nb_{15}:Cr_{40}:Pt_{45}, Sample 2: The nominal Nb_{15}:Cr_{15}:Pt_{70} alloy had a mainly single phase microstructure of (Pt) grains of different orientations, whereas nominal Nb_{15}:Cr_{40}:Pt_{45} comprised cored (Pt) dendrites.

Nominal Nb_{40}:Cr_{15}:Pt_{45}, Sample 3: The nominal Nb_{40}:Cr_{15}:Pt_{45} alloy had a complex microstructure of mainly cored ~$Nb_{1-X}Pt_{1+X}$ dendrites and a two ternary phases, τ5 and τ4, as shown in Figure 5 . In a small part near the edge, although the overall composition was very similar, and there were needles (which formed first) and dendrites (which formed next) (Figure 6). These were assumed to be the same phase, although they had different morphologies at slightly different compositions. The composition of the needles was closer to the binary, but the phases analyses of both appeared to be contiguous. The last phases were formed in peritectic reactions, and these were very small, making accurate analysis difficult.

Nominal Nb_{15}:Cr_{70}:Pt_{15}, Sample 4: The nominal Nb_{15}:Cr_{70}:Pt_{15} alloy microstructure comprised mainly (Cr) dendrites, with ~$NbCr_2$ and then τ1, as shown in Figure 7, formed with peritectic reactions.

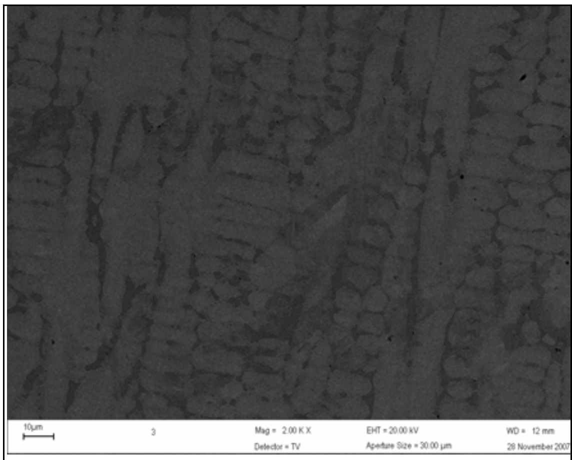

Figure 5. SEM-BSE image of the major part of nominal Nb_{40}:Cr_{15}:Pt_{45}, showing light ~$Nb_{1-X}Pt_{1+X}$ dendrites and dark τ5 and τ4 interdendritic phases.

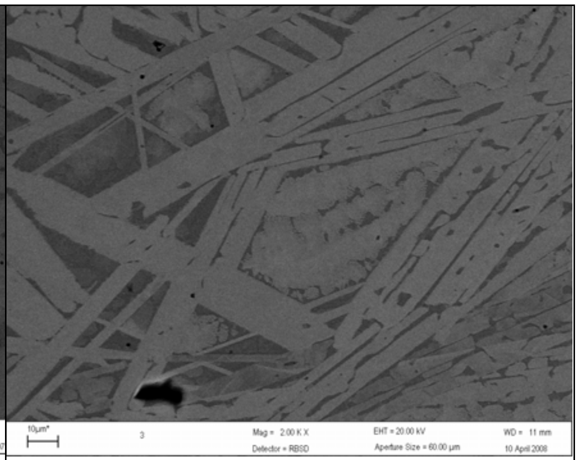

Figure 6. SEM-BSE image of the minor edge region of nominal Nb_{40}:Cr_{15}:Pt_{45}, showing light ~$Nb_{1-X}Pt_{1+X}$ needles and dendrites, with medium-grey τ5 and dark τ4 phase.

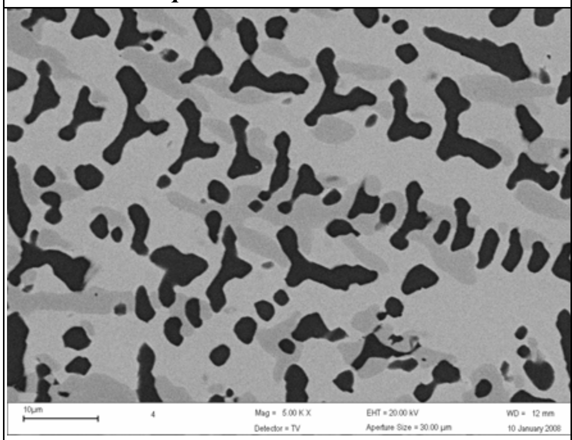

Figure 7. SEM-BSE image of nominal Nb_{15}:Cr_{70}:Pt_{15}, showing dark (Cr) dendrites, medium-grey ~$NbCr_2$ and light τ1 phases.

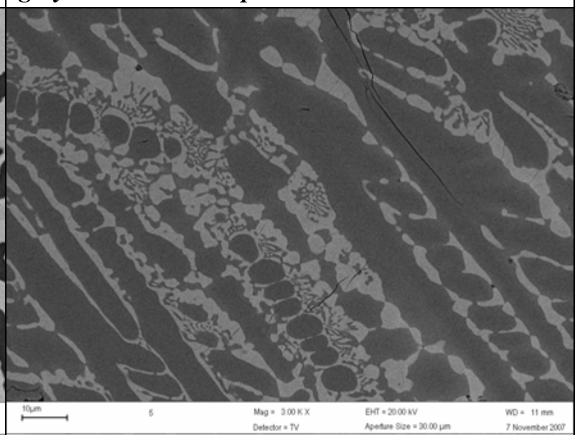

Figure 8. SEM-BSE image of nominal Nb_{40}:Cr_{45}:Pt_{15}, showing dark ~$NbCr_2$ dendrites, with a sparse eutectic of ~$NbCr_2$ + ~Nb_2Pt (light).

Nominal Nb_{40}:Cr_{45}:Pt_{15}, Sample 5: The nominal Nb_{40}:Cr_{45}:Pt_{15} alloy was quite brittle with cracks. This alloy comprised ~$NbCr_2$ dendrites and a ~Nb_2Pt interdendritic phase, with a sparse eutectic of ~$NbCr_2$ + ~Nb_2Pt, as shown in Figure 8.

Nominal Nb_{70}:Cr_{15}:Pt_{15}, Sample 6: The nominal Nb_{70}:Cr_{15}:Pt_{15} alloy possessed mainly (Nb) dendrites, with a cored ~Nb_3Pt matrix and small regions of a ~Nb_3Pt + ~$NbCr_2$ eutectic, as shown in Figure 9. The dendrites had ragged edges showing a peritectic reaction. Extrapolating through the eutectic overall from ~Nb_3Pt, which was one of the components, indicated that the second component was ~$NbCr_2$. There were high experimental errors for eutectic overall because of its small size areas. There were also high errors for the light matrix because of coring, and for medium-grey dendrites because of their small size.

Nominal Nb_{30}:Cr_{10}:Pt_{60}, Sample 7: The microstructure of nominal Nb_{30}:Cr_{10}:Pt_{60} was mainly ~$\beta NbPt_3$ needles, surrounded by cored (Pt).

Nominal Nb_{60}:Cr_{10}:Pt_{30}, Sample 8: Figure 10 shows nominal Nb_{60}:Cr_{10}:Pt_{30} alloy microstructure, which comprised ~Nb_3Pt dendrites, cored ~Nb_2Pt and τ5 phases; some of the phases were too small to analyse accurately.

Nominal Nb_{24}:Cr_{23}:Pt_{53}, Sample 9: The nominal Nb_{24}:Cr_{23}:Pt_{53} alloy possessed a microstructure of mainly ~$NbPt_2$ dendrites, and cored (Pt), with some porosity.

Nominal Nb_{50}:Cr_{30}:Pt_{20}, Sample 10: The nominal Nb_{50}:Cr_{30}:Pt_{20} sample had many cracks, and was very inhomogeneous, with both unmelted Pt and Nb regions. This alloy was analysed in different parts. A region near the unmelted Pt comprised ~$Nb_{1-X}Pt_{1+X}$ needles in a ~Nb_2Pt and τ4 matrix (Figure 11). Another nearby region had ~$Nb_{1-X}Pt_{1+X}$ dendrites and needles, with τ4 as a matrix (Figure 12). Along the sample edges, there were regions of ~$NbCr_2$ dendrites, with a binary eutectic ~$NbCr_2$ + ~Nb_2Pt, and a ternary eutectic ~$NbCr_2$ + ~Nb_2Pt + τ4 (Figure 13). Other regions had ~Nb_2Pt dendrites, surrounded by τ4 and interdendritic ~$NbCr_2$ (Figure 14); or ~$NbCr_2$ dendrites surrounded τ2 with ~Nb_2Pt and τ4 interdendritic phases (Figure 15).

Nominal Nb_{35}:Cr_{30}:Pt_{35}, Sample 11: The nominal Nb_{35}:Cr_{30}:Pt_{35} alloy comprised mainly cored (Pt) dendrites, with interdendritic τ2, which was too small to analyse accurately, and some porosity.

Nominal Nb_{20}:Cr_{50}:Pt_{30}, Sample 12: The nominal Nb_{20}:Cr_{50}:Pt_{30} alloy had some pores, and comprised mainly (Pt) dendrites surrounded by a (Pt) + τ1. eutectic, as shown in Figure 16.

Nominal Nb_{30}:Cr_{20}:Pt_{50}, Sample 13: The nominal Nb_{30}:Cr_{20}:Pt_{50} alloy had ~$NbPt_2$ dendrites with interdendritic τ3 (Figure 17), and some pores.

Nominal Nb_{25}:Cr_{45}:Pt_{30}, Sample 14: The nominal Nb_{25}:Cr_{45}:Pt_{30} alloy was inhomogeneous, with unmelted pure platinum and different microstructures. Three different regions were analysed individually, and were τ2 dendrites with interdendritic (Pt) as shown in Figure 18; and elsewhere (Pt) dendrites with interdendritic τ2; and also a sparse (Pt) + τ2 eutectic.

Nominal Nb_{20}:Cr_{60}:Pt_{20}, Sample 15: The nominal Nb_{20}:Cr_{60}:Pt_{20} alloy had unmelted regions of all the constituents. It was inhomogeneous and was analysed as different parts. The major portion was similar to Sample 4. A region near the unmelted Nb comprised τ1 dendrites with interdendritic (Pt). Another region had τ1 dendrites, with a τ1 + ~Cr_3Pt eutectic (Figure 19).

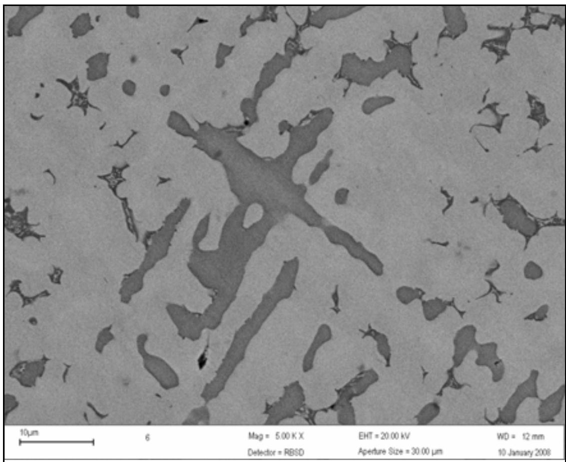

Figure 9. SEM-BSE image of nominal Nb_{70}:Cr_{15}:Pt_{15}, showing medium (Nb) dendrites, light ~Nb_3Pt matrix and a ~Nb_3Pt + ~$NbCr_2$ eutectic reaction.

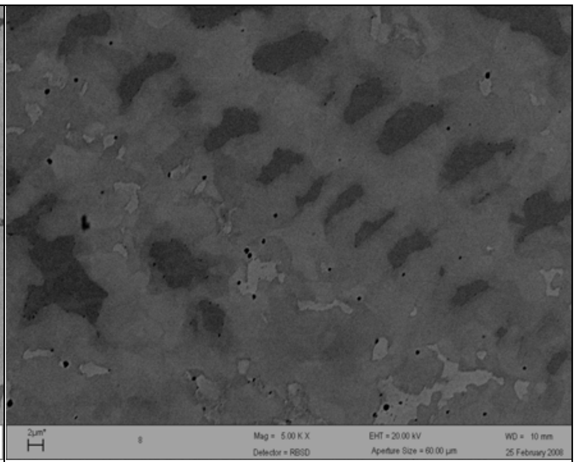

Figure 10. SEM-BSE image of nominal Nb_{60}:Cr_{10}:Pt_{30}, showing dark ~Nb_3Pt dendrites, medium-grey ~Nb_2Pt and light τ5 phases.

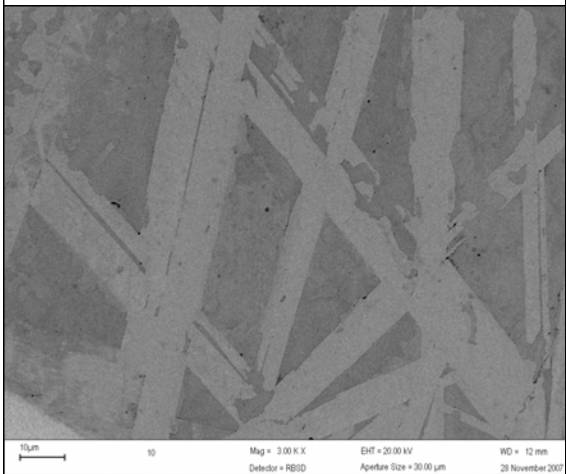

Figure 11. SEM-BSE image of nominal Nb_{50}:Cr_{30}:Pt_{20} alloy in the as–cast condition, showing light $Nb_{1-X}Pt_{1+X}$ needles, a medium-grey ~Nb_2Pt and dark τ4 phases between the needles.

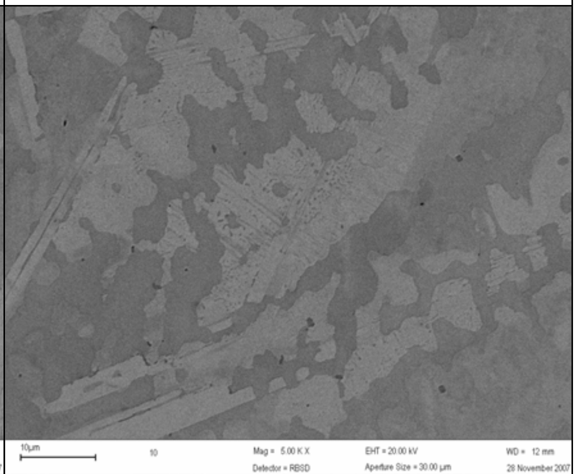

Figure 12. SEM-BSE image of nominal Nb_{50}:Cr_{30}:Pt_{20}, showing light ~$Nb_{1-X}Pt_{1+X}$ dendrites, medium-grey τ4 interdendritic and a light τ5 mixture of dendrites and needles phases.

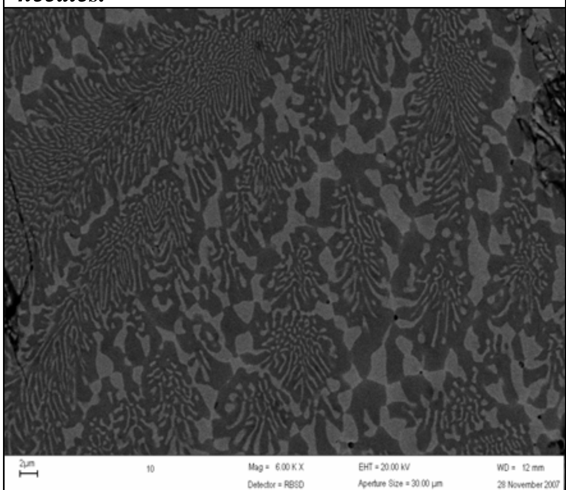

Figure 13. SEM-BSE image of nominal Nb_{50}:Cr_{30}:Pt_{20} , showing fine binary ~$NbCr_2$ (dark) + ~Nb_2Pt (light) eutectic and coarse ternary ~$NbCr_2$ + ~Nb_2Pt + τ4 (very light)

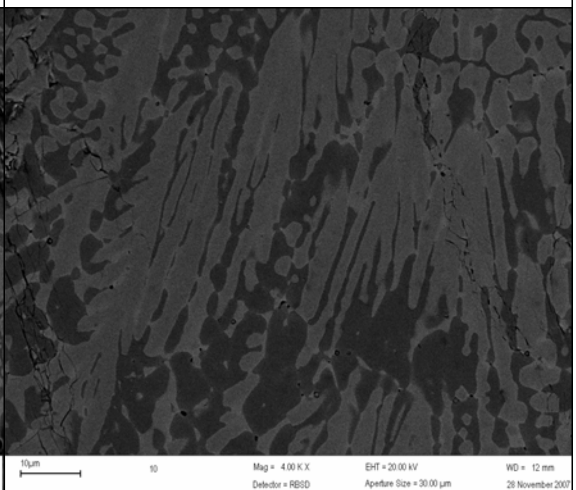

Figure 14. SEM-BSE image of nominal Nb_{50}:Cr_{30}:Pt_{20}, showing medium-grey ~Nb_2Pt dendrites, light τ4 and dark ~$NbCr_2$ interdendritic phase.

Nominal Nb_{35}:Cr_{40}:Pt_{25}, Sample 16: The nominal Nb_{35}:Cr_{40}:Pt_{25} alloy had unmelted Pt, with two different regions and was cracked. One region had ~$NbCr_2$ dendrites, in a matrix of τ4 and τ2. In another region, there were τ2 dendrites with τ3 and lines of pores interdendritically, as shown in Figure 20.

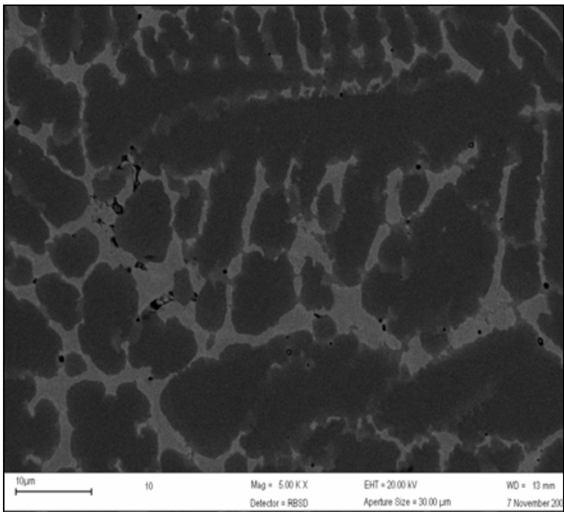

Figure 15. SEM-BSE image of nominal Nb_{50}:Cr_{30}:Pt_{20}, showing dark ~$NbCr_2$ dendrites, and light ~Nb_2Pt and τ4 interdendritic phase.

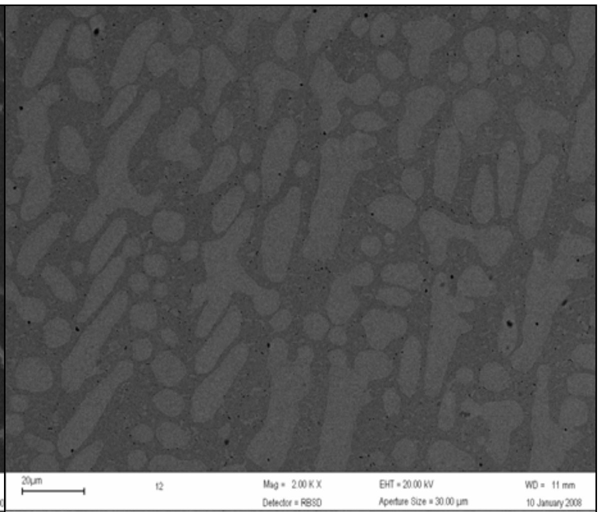

Figure 16. SEM-BSE image of nominal Nb_{20}:Cr_{50}:Pt_{30}, showing light (Pt) dendrites and (Pt) + τ1 eutectic.

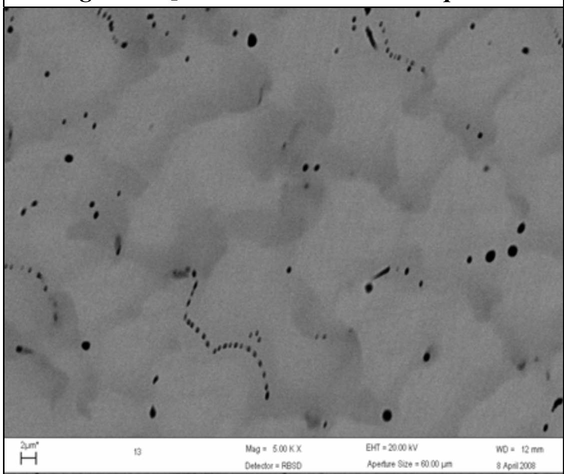

Figure 17. SEM-BSE image of nominal Nb_{30}:Cr_{20}:Pt_{50}, showing light ~$NbPt_2$ dendrites and a medium-grey τ3 phase.

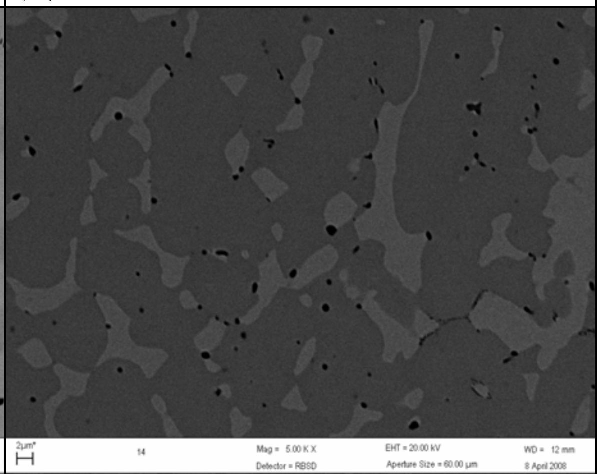

Figure 18. SEM-BSE image for the major part, near the edge in nominal Nb_{25}:Cr_{45}:Pt_{30}, showing medium-grey τ2 dendrites and light (Pt) interdendritic phase.

Nominal Nb_{40}:Cr_{25}:Pt_{35}, Sample 17: The nominal Nb_{40}:Cr_{25}:Pt_{35} alloy microstructure comprised mainly τ3 dendrites with very irregular edges and cored τ4, as shown in Figure 21.

Nominal Nb_{57}:Cr_{18}:Pt_{25}, Sample 18: Nominal Nb_{57}:Cr_{18}:Pt_{25} had unmelted Nb and was homogeneous away from the unmelted Nb. The microstructure comprised τ4 dendrites, with ~Nb_2Pt on the edges and interdendritic ~$NbCr_2$, as shown in Figure 22.

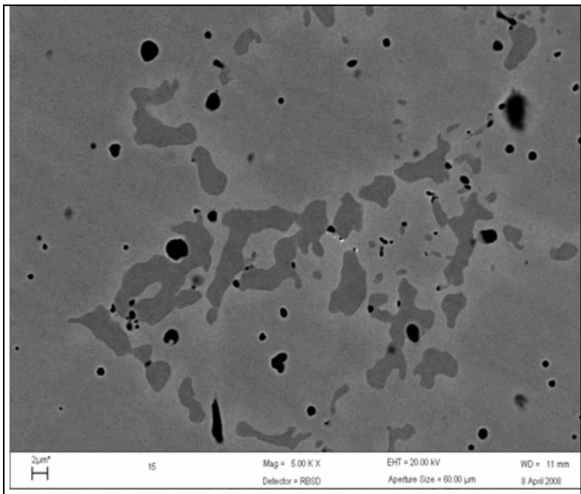

Figure 19. SEM-BSE image for the major region near the unmelted Nb in nominal Nb_{20}:Cr_{60}:Pt_{20}, showing medium-grey τ1 dendrites and dark ~Cr_3Pt phase.

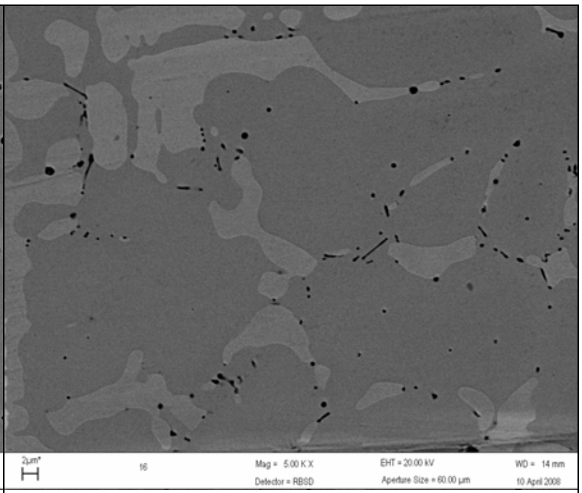

Figure 20. SEM-BSE image for the minor part near the unmelted Pt in nominal Nb_{35}:Cr_{40}:Pt_{25}, showing medium-grey τ4 dendrites and light τ3 interdendritic phase.

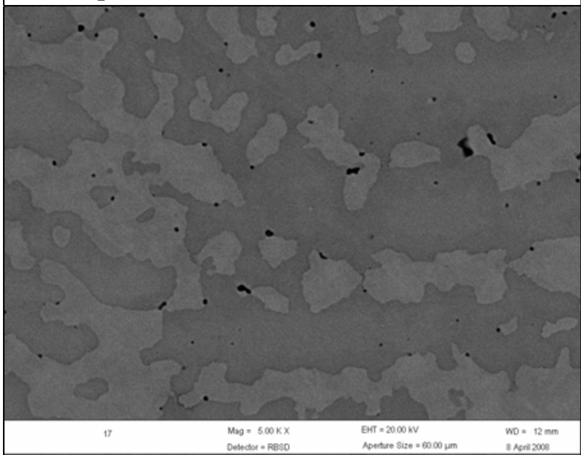

Figure 21. SEM-BSE images of nominal Nb_{40}:Cr_{25}:Pt_{35}, showing light τ3 dendrites and medium-grey τ4 interdendritic phase.

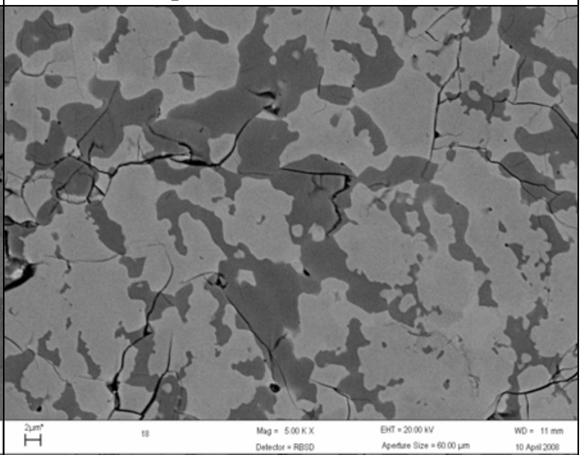

Figure 22. SEM-BSE image of nominal Nb_{57}:Cr_{18}:Pt_{25}, showing medium-grey τ4 dendrites, light ~Nb_2Pt and dark ~$NbCr_2$.

4.2 Mechanical properties

4.2.1 Hardness

The results of the Vickers macrohardness tests are presented in Table 2.

Table 2. Macrohardness measurements of ternary Nb-Cr-Pt alloys using a 5kg load.

Sample name	**Alloy composition (at.%)**	**Hardness (HV_5)**	**Phases**	**Cracks?**	**Ductile/Brittle**
1	Nb_{15}:Cr_{15}:Pt_{70}	716±51	(Pt)	No cracks	Ductile
2	Nb_{15}:Cr_{40}:Pt_{45}	642±20	(Pt)	No cracks	Ductile
3	Nb_{40}:Cr_{15}:Pt_{45}	601±8	~$Nb_{1-X}Pt_{1+X}$, ~Nb_2Pt, τ4 and τ5	No cracks	Ductile
4	Nb_{15}:Cr_{70}:Pt_{15}	783±109	(Cr), ~$NbCr_2$, τ1, ~Nb_3Pt and (Nb)	Corner cracks	Brittle
5	Nb_{40}:Cr_{45}:Pt_{15}	738±63	~$NbCr_2$ and ~Nb_2Pt	Corner cracks	Brittle
6	Nb_{70}:Cr_{15}:Pt_{15}	762±93	(Nb), ~Nb_3Pt and ~$NbCr_2$	Corner cracks	Brittle
7	Nb_{30}:Cr_{10}:Pt_{60}	527±24	~β$NbPt_3$ and (Pt)	Minor cracks	Ductile/brittle
8	Nb_{60}:Cr_{10}:Pt_{30}	745±102	~Nb_3Pt, ~Nb_2Pt and τ5	Corner cracks	Brittle
9	Nb_{24}:Cr_{23}:Pt_{53}	456±19	~$NbPt_2$ and (Pt)	No cracks	Ductile
10 Local regions	Nb_{44}:Cr_{12}:Pt_{44} $Nb_{40.3}$:$Cr_{20.1}$:$Pt_{39.6}$	332±91	~$Nb_{1-X}Pt_{1+X}$, ~Nb_2Pt, τ4 and τ5	Minor cracks	Brittle/ductile
	$Nb_{44.1}$:$Cr_{34.1}$:$Pt_{21.9}$	507±84	~Nb_2Pt, ~$NbCr_2$ and τ4	Corner cracks	Brittle
	$Nb_{42.5}$:$Cr_{38.6}$:$Pt_{18.9}$	795±0	~Nb_2Pt, ~$NbCr_2$ and τ4	Corner cracks	Brittle
	$Nb_{41.5}$:$Cr_{39.8}$:$Pt_{18.8}$	795±0	~Nb_2Pt, ~$NbCr_2$ and τ4	Corner cracks	Brittle

	$Nb_{39.3}$:$Cr_{42.4}$:$Pt_{18.3}$	795±0	~Nb_2Pt, ~$NbCr_2$ and τ4	Corner cracks	Brittle
	Unmelted Pt	113±16	Pt	No cracks	Ductile

Table 2. (Continued).

11	Nb_{35}:Cr_{30}:Pt_{35}	642±8	(Pt) and τ2	Minor cracks	Ductile/Brittle
12	Nb_{20}:Cr_{50}:Pt_{30}	739±14	(Pt) and τ1	Minor cracks	Ductile/Brittle
13	Nb_{30}:Cr_{20}:Pt_{50}	655±8	~$NbPt_2$ and τ3	Minor cracks	Ductile/Brittle
14	Nb_{25}:Cr_{45}:Pt_{30}	934±26	(Pt) and τ2	Corner cracks	Brittle
15 Local regions	$Nb_{13.1}$:$Cr_{70.1}$:$Pt_{16.8}$	966±35	(Cr), ~Cr_3Pt and τ1	Corner cracks	Brittle
	$Nb_{17.6}$:$Cr_{60.5}$:$Pt_{21.9}$ $Nb_{16.6}$:$Cr_{63.0}$:$Pt_{20.4}$	511±15	(Pt), ~Cr_3Pt and τ1	Minor corner cracks	Brittle/ductile
17	Nb_{40}:Cr_{25}:Pt_{35}	936±67	τ3 and τ4	Corner cracks	Brittle/ductile
18	Nb_{57}:Cr_{18}:Pt_{25}	870±79	~Nb_2Pt, ~$NbCr_2$ and τ4	Corner cracks	Brittle

4.2.2 Toughness

In order to obtain a qualitative evaluation of the alloys' toughness, photographs were taken of the hardness indentations. Cracking around an indentation in an indication of brittleness, while the slip mode around the indentations shows whether the alloy has reasonable toughness (planar slip) or even better resistance against cracking (wavy slip). Figure 23 gives examples of the different toughnesses, showing the relevant hardness indentations and slip modes. Nominal Nb_{15}:Cr_{40}:Pt_{45} and Nb_{24}:Cr_{23}:Pt_{53} showed wavy slip, indicating their plastic deformation. Brittleness was observed in nominal Nb_{15}:Cr_{70}:Pt_{15} showing cracks, and also in nominal Nb_{40}:Cr_{45}:Pt_{15} which had major cracking.

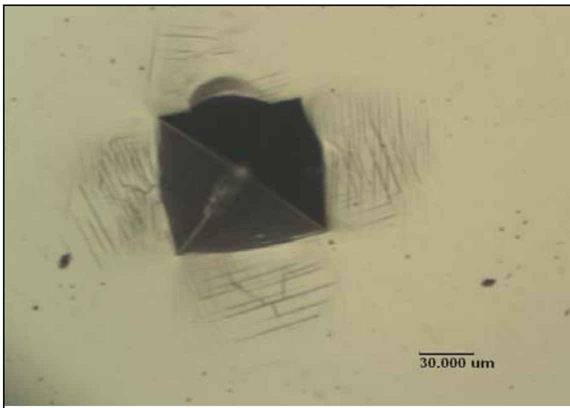

Nominal Nb_{15}:Cr_{40}:Pt_{45} showing wavy slip

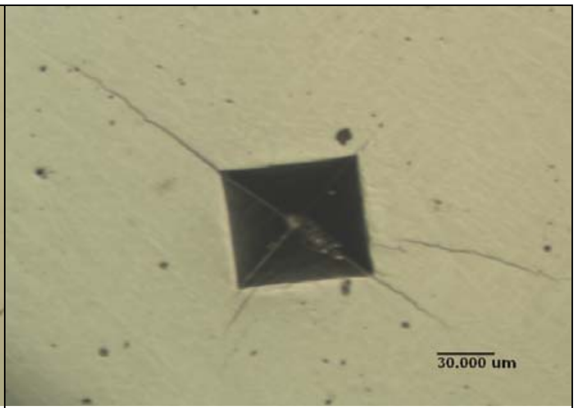

Nominal Nb_{15}:Cr_{70}:Pt_{15} showing cracking

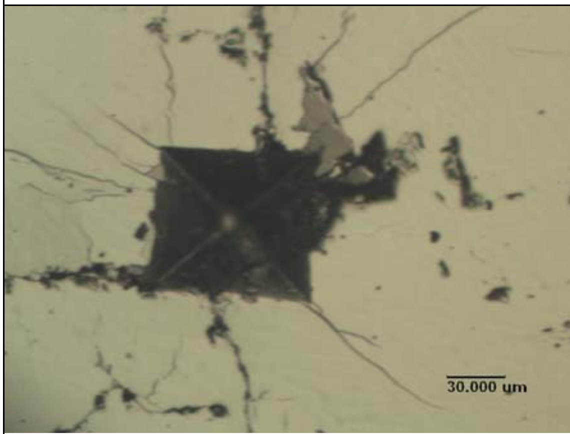

Nominal Nb_{40}:Cr_{45}:Pt_{15} showing major cracking

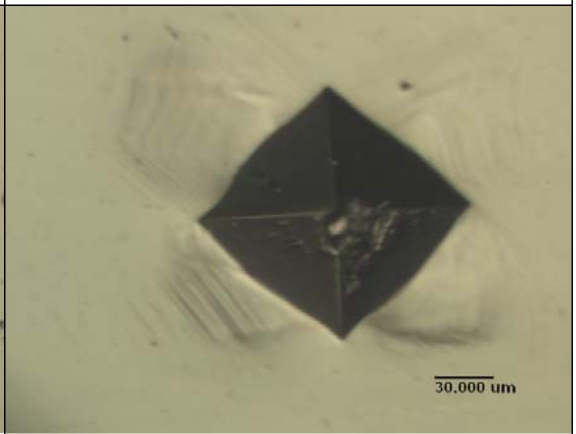

Nominal Nb_{24}:Cr_{23}:Pt_{53} showing wavy slip

Figure 23. Optical micrographs showing macrohardness indentations of selected as-cast Nb-Cr-Pt alloys.

5. Discussion

5.1 Phase investigations and solidification projection for the Nb-Cr-Pt system

Using analyses from reasonable phase sizes (where possible, greater than 3µm) and with good reproducibility, the best phase results were plotted. All binary phases were found to extend into the ternary, except for α′Pt, which was not identified. Five ternary phases were identified on the basis of the phase contrasts in the microstructures (Figures 4–22) and the fact that the plotted compositions could not be an extension of a binary phase because that binary phase was already present in a sample. The different compositions for the phases were then joined to give the solidification projection shown in Figure 24. The (Pt) binary phase was found to have the largest extent.

The τ1 composition of nominal ~Nb_{20}:Cr_{50}:Pt_{30} (Alloy 12) was obtained by extrapolation through the eutectic overall from (Pt), taking a 50/50 proportion of the (Pt) + τ1 eutectic. The τ2 ternary phase was found near to nominal ~Nb_{25}:Cr_{45}:Pt_{30} (Alloy 14) and ~Nb_{35}:Cr_{40}:Pt_{25} (Alloy 16). The τ5 phase was identified in nominal ~Nb_{40}:Cr_{15}:Pt_{45} (Alloy 3), ~Nb_{60}:Cr_{10}:Pt_{30} and locally in Alloy 10 at regions of overall compositions ~$Nb_{40.3}$:$Cr_{20.1}$:$Pt_{39.6}$ and ~$Nb_{44.1}$:$Cr_{34.1}$:$Pt_{21.9}$.

XRD Peaks at 2θ = 38°, 48°, 55° and 56° from nominal ~Nb_{30}:Cr_{20}:Pt_{50} (Alloy 13), ~Nb_{35}:Cr_{40}:Pt_{25} (Alloy 16) and ~Nb_{40}:Cr_{25}:Pt_{35} (Alloy 17) are deduced to be from τ3.

The extensions of the binary phases were determined as:

- (Cr): a least ~2 at.% Nb;
- (Pt), (Nb), ~$NbPt_2$ and ~$NbCr_2$ extend ~20 at.% into the ternary;
- ~Cr_3Pt: ~10 at.% Nb;
- ~$\beta NbPt_3$: ~4 at.% Cr;
- ~$Nb_{1-X}Pt_{1+X}$: ~13 at.% Cr;
- ~Nb_3Pt: ~10 at.% Cr;
- ~Nb_2Pt: ~26 at.% Cr.

The ternary phases and their approximate compositions are:

- τ1: ~Nb_{17}:Cr_{64}:Pt_{19};
- τ2: ~Nb_{28}:Cr_{55}:Pt_{17};
- τ3: ~Nb_{30}:Cr_{30}:Pt_{40};
- τ4: ~Nb_{45}:Cr_{27}:Pt_{28};
- τ5: ~Nb_{40}:Cr_{18}:Pt_{42}.

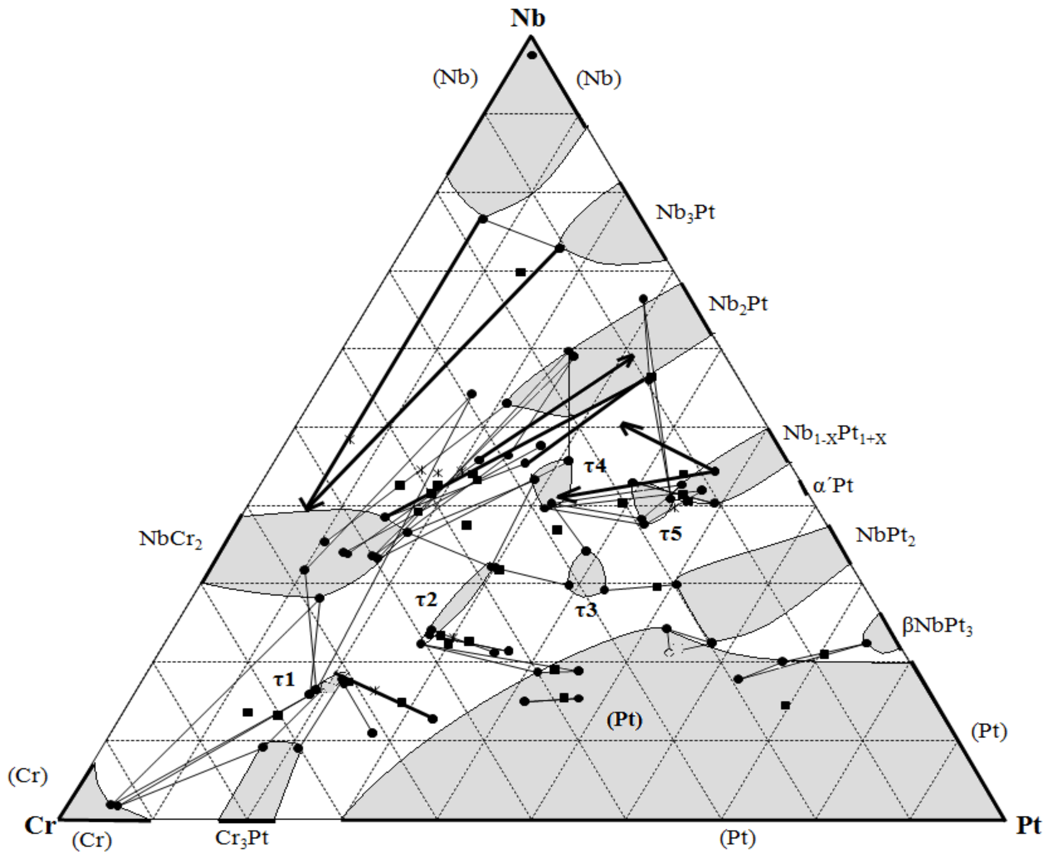

Figure 24. Solidification projection diagram of the Nb-Cr-Pt system.

5.2 Mechanical properties of the ternary Nb-Cr-Pt alloys

5.2.1 Hardness

The average Vickers macrohardness measurements are superposed on the solidification projection in Figure 25.

The main findings of the investigation into the hardness of the Nb-Cr-Pt alloys were:

- Alloys in the (Pt)-rich region were ductile with no cracks on the indentations.
- All the Nb-Cr-Pt alloys containing > 40 at.% Pt had low hardnesses, and were mostly ductile.
- Samples with high chromium and niobium contents had high hardnesses, and were extremely brittle.
- Three alloys had extremely high hardnesses, around ~945 (HV_5). One alloy had a three-phase region of (Cr) + ~Cr_3Pt + τ1, with the other two alloys having two-phase regions of (Pt) + τ2 and τ3 + τ4.
- Alloys which had eutectics were mostly brittle, except where there was a (Pt) solid solution (Alloy 12).

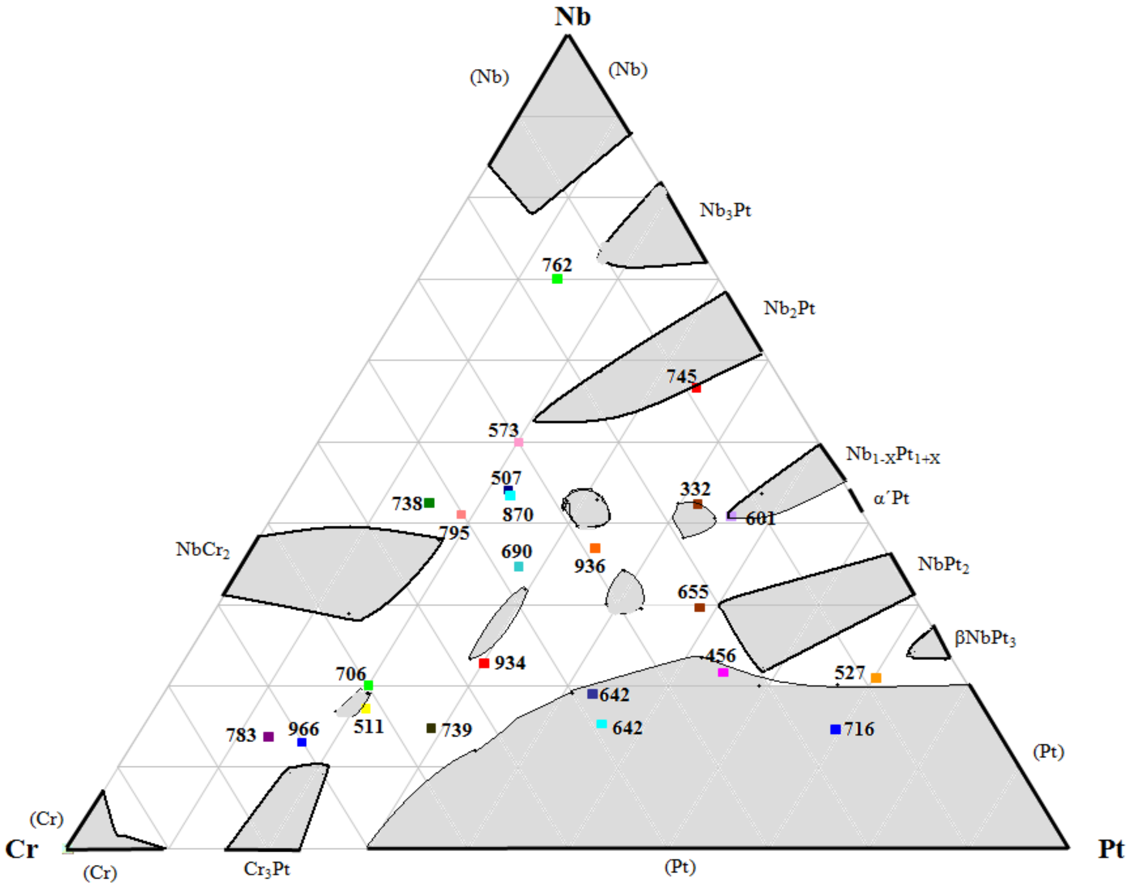

Figure 25. Vickers macrohardnesses of the ternary Nb-Cr-Pt alloys.

5.2.2 Toughness

The different slip modes of the as-cast Nb-Cr-Pt alloys are superposed on the solidification projection in Figure 26 and the mechanical behaviour is plotted in Figure 27.

Alloys with a single phase (Pt) showed planar or wavy slip. The alloys with about ≥ 45 at.% Pt exhibited planar, wavy or wavy and minor cracks slip mode, while the ones with ≤ 20 at.% Pt had cracks, showing their brittleness. Around all the newly identified ternary phases, all slip behaviours (planar and wavy) were observed with cracks. Alloys with (Pt) and ~$NbPt_2$ phases were found to have good toughness.

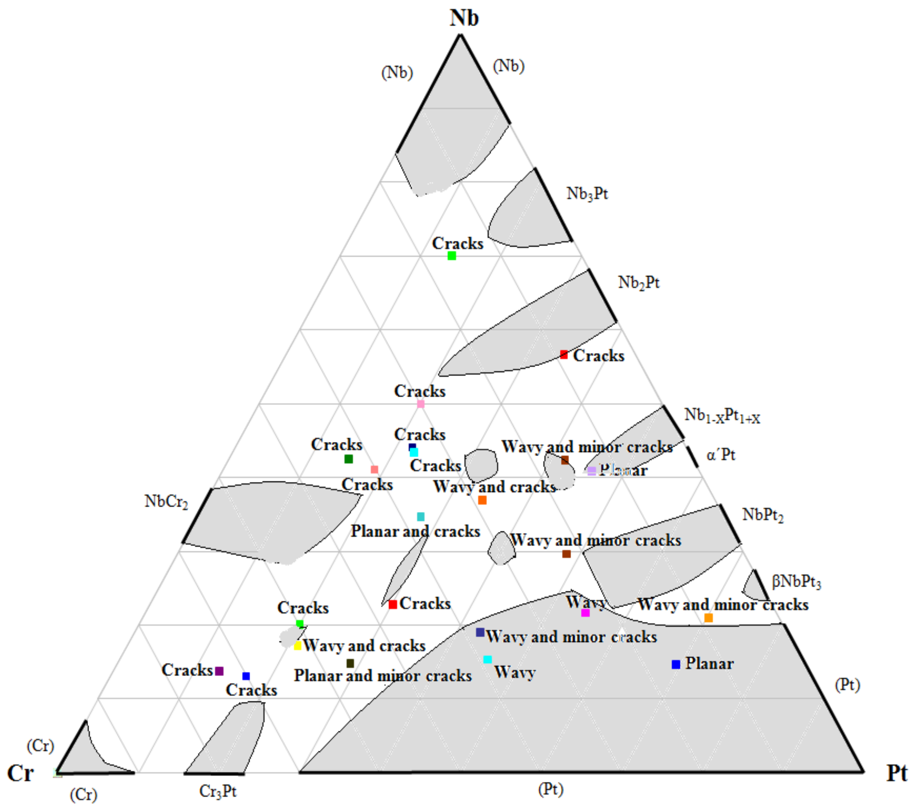

Figure 26. Summary of the slip modes of as-cast Nb-Cr-Pt alloys, superposed on the solidification projection.

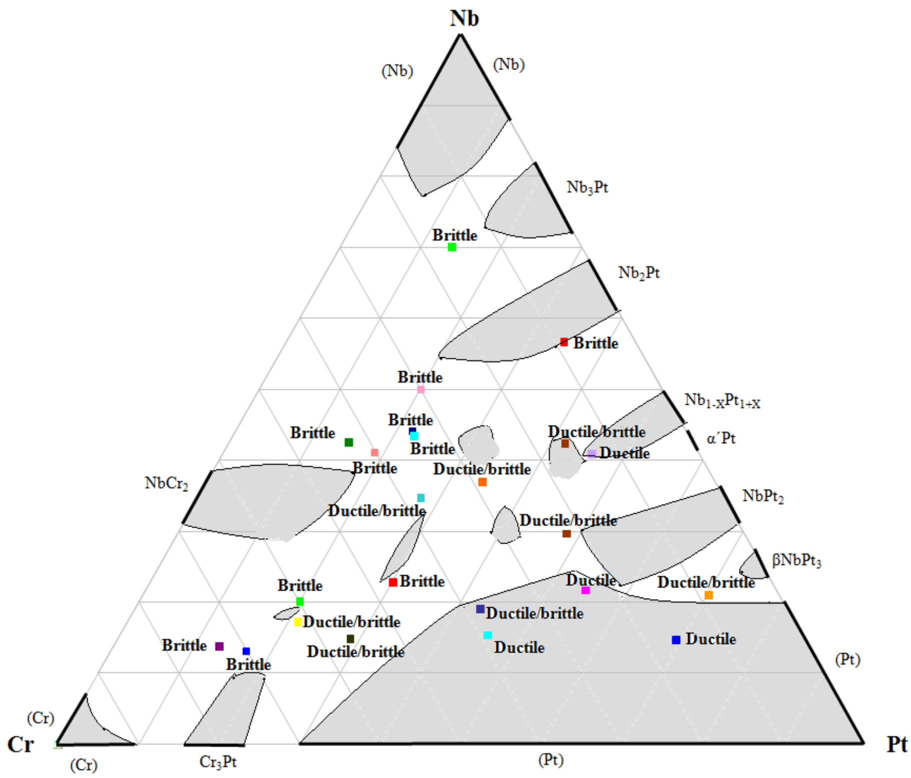

Figure 27. Summary of the mechanical behaviour of the as-cast Nb-Cr-Pt alloys, superposed on the solidification projection.

6. Conclusions

Eighteen samples of different compositions were studied using SEM with EDX and the phases were mainly confirmed by X-ray diffraction (XRD). A solidification projection was drawn, showing the extent of the phases into the ternary. Five ternary phases were identified. Hardness measurements were undertaken, and alloys with (Pt) and ~$NbPt_2$ phases were found to have good mechanical properties, being ductile with reasonable hardness. Alloys containing (Cr), (Nb), ~Cr_3Pt, ~$NbCr_2$, ~Nb_3Pt and ~Nb_2Pt were extremely brittle with cracks.

7. Acknowledgements

The authors would like to thank Mintek, the DST/NRF Centre of Excellence in Strong Materials and the Platinum Development Initiative (PDI) for support.

8. References

[1986Mis] Y. Mishima, Y. Oya and T. Suzuki, Proceedings of the International Conference on Martensitic Transformations, Japan Institute of Metals, (1986), p. 1009–1014.

[1987Sim] C.T. Sims, N.S. Stoloff and W.C. Hagel, Superalloys II: High Temperature Materials for Aerospace and Industrial Power, Wiley–Interscience, USA, (1987).

[1990Mas] T.B. Massalski, Binary Alloy Phase Diagrams, ASM International, (1990), Ohio, USA.

[1992Tho] D.J. Thoma and J.H. Perepezko, *Mat. Sci. & Eng.*, A156, (1992), pp. 97–108.

[1993Oka] H. Okamoto, *J. of Phase Equilibria*, 14(4), (1993).

[2000Com1] D.N. Compton, L.A. Cornish and M.J. Witcomb, Microscopy and Microanalysis 2000, volume 6, Supplement 2, 370 – 371, Philadelphia, Pennsylvania, USA, 13th – 17th August 2000.

[2000Com2] D.N. Compton, L.A. Cornish and M.J. Witcomb, Proc. Microsc. Soc. south. Afri. , Vol. 30, p. 9, Grahamstown, 6th – 8th December 2000.

[2000Wol] I.M. Wolff and P.J. Hill, *Plat. Metals Rev.*, 44, (4), (2000), pp. 158–166.

[2001Com] D.N. Compton, L.A. Cornish, and M.J. Witcomb, Microscopy and Microanalysis 2001, Vol. 7, Supplement 2, 1248–1249, Pub. Springer–Verlag, NY, Inc. , Long Beach, California, USA, 5th – 9th August 2001.

[2001Hil] P.J. Hill, Superalloy Analogues Based on Platinum for Ultra–High Temperature Applications, PhD Thesis, University of Witwatersrand, Johannesburg, South Africa, (2001).

[2001Süs] R. Süss, P.J. Hill, P. Ellis and L.A. Cornish, Proc. Microsc. Soc. south. Afr., Vol. 31, p. 21, Johannesburg, 5–7th December 2001.

[2002Cor] L.A. Cornish, J. Hohls, P.J. Hill, S.N. Prins, R. Süss and D.N. Compton, *J. Mining and Metallurgy*, 38 ((3–4) B) (2002), pp. 197–204.

[2002Süs1] R. Süss, L.A. Cornish, L. Glaner and D.N. Compton, ICEM 15, Proceedings of the 15th international Congress on Electron Microscopy, 1st – 6th September 2002, Durban, South Africa.

[2002Süs2] R. Süss, R. Völkl, D. Freund, B. Fischer, P.J. Hill, P. Ellis and I.M. Wolff, *Mat. Sci. & Eng.*, A338, (2002), pp. 133–141.

[2003Cho] L.H. Chown and L.A. Cornish, Proc. 2nd International Conference of the African Materials Society, Johannesburg, (2003), pp. 136–137.

[2003Cor] L.A. Cornish, B. Fischer and R. Völkl, *Mat. Res. Bul.*, 28 (9) (2003), pp. 632–638.

[2003Gla] L. Glaner and L.A. Cornish, Proc. Microsc. Soc. south. Afr., Vol. 33, (2003), p. 17.

[2003Hua] C. Huang, Y. Yamabe-Mitarai, K. Nishida and H. Harada, Intermetallics, 11, (2003), pp. 917–926.

[2003Pri] S.N. Prins, The Al–Pt–Ru Ternary Phase Diagram, MSc Dissertation, University of Pretoria, Pretoria, South Africa, (2003).

[2003Süs1] R. Süss, L.A. Cornish and B. Joja, Proc. Microsc. Soc. south. Afri., Vol. 33, (2003), p.13.

[2003Süs2] R. Süss, U. Glatzel, S.N. Prins and L.A. Cornish, Proc. 2nd International conference of the African Materials Society, (2003), p. 141–142.

[2003Süs3] R. Süss, L.A. Cornish, P.J. Hill and J. Hohls, Proceedings of Advanced Materials and Processes of Gas Turbines, 22–26 September 2002, Copper Mountain, Colorado, USA, TMS, (2003), pp. 301–308.

[2004Hua1] C. Huang, Y. Yamabe–Mitarai and H. Harada, *J. Alloys & Compounds*, 366 (2004), pp. 217–221.

[2004Hua2] C. Huang, Y. Yamabe-Mitarai, S. Nakazawa and H. Harada, *Mat. Let.*, 58, (2004), pp. 483–488.

[2004Süs1] R. Süss, Investigation into the Pt–Cr–Ru System, MSc Dissertation, University of the Witwatersrand, Johannesburg, South Africa, (2004).

[2004Süs2] R. Süss, L.A. Cornish, L.H. Chown and L. Glaner, Beyond Ni-based Superalloys, TMS 2004 133rd Annual Meeting and Exhibition, Charlotte, North Carolina, USA, (2004), p. 269.

[2004Vor] S. Vorberg, M. Wenderoth, B. Fischer, U. Glatzel, and R. Völkl, *JOMs*, 56(9), (2004), pp. 40–43.

[2005Hua] C. Huang, Y. Yamabe-Mitarai, X.H. Yu, S. Nakazawa and H. Harada, *Met. & Mat. Trans.*, Vol. 36A, (2005), pp. 539–545.

[2005Wen] M. Wenderoth, L.A. Cornish, R. Süss, S. Vorberg, B. Fischer, U. Glatzel and R. Völkl, *Met. & Mat. Trans.*, Vol. 36A, (2005), pp. 567–575.

[2005Zha] J.-C. Zhao, X. Zheng and D.G. Cahil, *Materials Today*, October (2005), pp. 28–37.

[2006Ndl] G.F. Ndlovu, L.A. Cornish, A. Douglas, B.A. Julies and B. Joja, Proc. Microsc. Soc. south. Afr., Vol. 36, (2006), p.11.

[2007Dou] A. Douglas, J.H. Neethling, R. Santamarta, D. Schryvers and L.A. Cornish, *J. Alloys & Compounds*, 432, (2007), pp. 96–102.

[2007Ndl] G.F. Ndlovu, Microstructural Investigation of the Pt-Al-Nb System, MSc Dissertation, University of the Western Cape, Cape Town, South Africa, (2007).

[2008Sho] M.B. Shongwe, L.A. Cornish and R. Süss, Advanced Metals Initiative Conference, 18^{th}–19^{th} November 2008.

[2008Süs] R. Süss, Investigation of the Pt-Al-Cr system as part of the development of the Pt-Al-Cr-Ru thermodynamic database, PhD Thesis, University of the Witwatersrand, Johannesburg, South Africa, (2008).

[2008Ukp] A.M. Ukpong, L.A. Cornish, R. Süss and A. Watson, Advanced Metals Initiative Conference, 18^{th}–19^{th} November 2008.